Stacking order dependence of interlayer excitons in $MoSe_2/WSe_2$ heterobilayers

Jinyang Lou,[1,*] Zheng Lv,[1,*] Haochen Wang,[1] Yutao Tang,[2] Song Luo,[1] Yan Liu,[1] Xinyue Zhang,[1] Guoxing Lv,[1] Yuning Zhang,[1] Hang Zhou,[1] Long Zhang,[1,†] and Zhanghai Chen[1,‡]

[1]*Department of Physics, College of Physical Science and Technology, Xiamen University, Xiamen 361005, China*

[2]*Shenzhen Shanxi Coal Hi-tech Research Institute Co., Ltd., Shenzhen 518083, China*

(Received 8 February 2024; revised 15 June 2024; accepted 18 June 2024; published 8 July 2024)

Two-dimensional transition metal dichalcogenide heterostructures provide a unique opportunity for quantum engineering of electronic and excitonic states at the nanoscale. Critical optical properties of interlayer excitons, including transition energy, optical selectivity, and quantum yield, are strongly correlated to the stacking orders. However, these optical properties could vary from sample to sample, setting an obstacle to extracting the intrinsic stacking order dependence experimentally. We report an effective method to fabricate heterobilayers with both stacking orders obtained on a single device. The sharp difference of interlayer excitons induced by the stacking orders was unambiguously identified, including emission wavelength, valley polarization, and temperature dependence of quantum yield. This method provides a flexible platform to study stacking order dependence of heterobilayer excitons, and can be readily applied to explore the layer hybridization, strong correlations, and exciton diffusion that are sensitive to stacking order.

DOI: 10.1103/PhysRevB.110.045412

I. INTRODUCTION

Van der Waals heterostructures made of monolayer transition metal dichalcogenides (TMD) have emerged as a promising platform for exploring exotic excitonic and electronic states [1–5]. When two van der Waals materials are stacked together, the lattice mismatch and twist angle between them can generate a nanoscale moiré pattern, which will manipulate excitonic and electronic states in both single-particle [6–11] and many-body regimes [12–27].

When the twist angle is close to 0° or 60°, the heterobilayer will form two different stacking orders, known as *R* stacking and *H* stacking. There have been intensive studies on the twist angle dependence of moiré excitons within certain stacking orders, from which the continuous modulation of excitons is observed including energy [28,29], lifetime [30,31], and diffusion length [32,33]. Compared to the twist angle, stacking order will make an impact on the moiré excitons more significantly [9,34,35]. First of all, the interlayer coupling is strongly correlated to the stacking orders, resulting in moiré lattices with different potential landscapes and symmetries. Moreover, the spin configuration of interlayer optical transitions will be reversible for *R* and *H* stacking orders, which determines the Zeeman effect of interlayer excitons (IX) [8,36,37], spin conserved interlayer hybridization [38,39], and arrangement of spin singlet and triplet excitons [40,41]. Most recently, the quadrupolar excitons with nonlinear optical stark effect have been observed in trilayer structures with specific stacking orders [42–44]. Optical properties of moiré interlayer excitons in heterobilayers with *R* and *H* stacking orders have been studied in various combinations [8,45]. However, the comparison has been limited to different samples prepared separately, where the influence of strain, dielectric environment, and crystal quality cannot be avoided, setting an obstacle to extract the intrinsic stacking order dependence of optical properties for moiré excitons.

Here, we report an effective method to prepare heterobilayers with both stacking orders in a single $MoSe_2/WSe_2$ heterobilayer, which provides a uniform condition to study moiré interlayer excitons from the heterobilayer with *R* and *H* stacking orders in parallel, including the emission energy, optical selectivity, and magnetic *g* factors. We also find that the quantum yield of interlayer excitons from two stacking orders exhibits a sharp difference, which results from the opposite energy alignment between spin singlet and triple excitons. Such a conclusion provides understanding of the heterobilayer as gain material for interlayer exciton lasers [57–59]. Our findings provide an effective platform to study moiré excitons and offer additional opportunities to investigate and engineer the valleytronics in bilayers. Future works are expected to explore stacking order dependence of other novel optical phenomena, such as interlayer hybridization [9,29,39,46], moiré lattice reconstruction [11,47,48], and strongly correlated states of electrons and excitons [2–5,14,24,49].

II. FABRICATION OF THE HETEROBILAYER

As shown in Fig. 1(a), to achieve both the *R*-type and *H*-type stacking configurations in one uniform heterostructure, monolayers from *A* and *B* layers of the 2*H* phase TMD bilayers (WSe_2 in this schematic) need to be isolated separately. Interestingly, such a monolayer-bilayer-monolayer sample can be obtained by mechanical exfoliation. As shown by the microscopic image of the exfoliated WSe_2 crystal in Fig. 1(b), there are two discontinuous regions of monolayers

*These authors contributed equally to this work.
†Contact author: zhanglong@xmu.edu.cn
‡Contact author: zhanghai@xmu.edu.cn

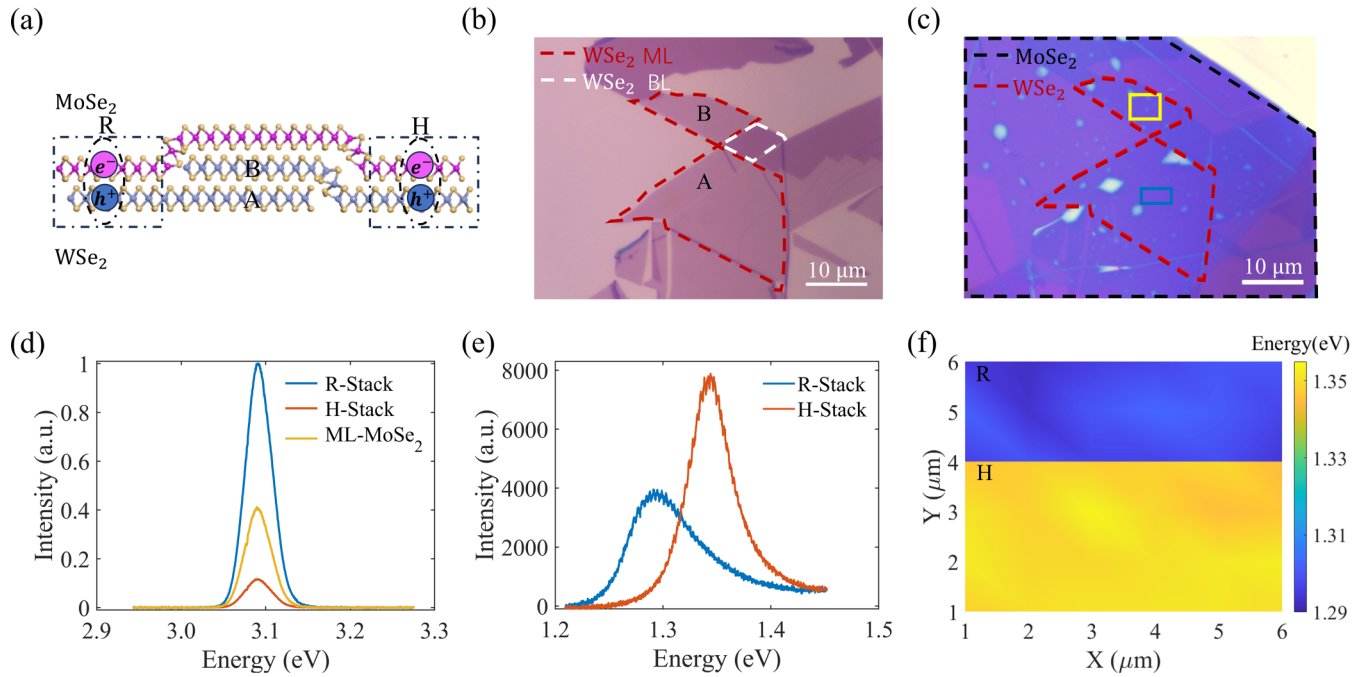

FIG. 1. $MoSe_2/WSe_2$ heterostructure and interlayer excitons. (a) Schematic of the heterostructures composed of a $MoSe_2$ monolayer and a WSe_2 homobilayer. The bottom (*A*) and top (*B*) layer of the WSe_2 homobilayer are isolated, forming the heterobilayer with *R* and *H* stacking orders, respectively, indicated by the dashed boxes. (b) Optical micrograph of the WSe_2 layer on SiO_2/Si substrate. The regions labeled by red dashed lines correspond to *A* and *B* layers, and the bilayer region is indicated by the white dashed line. (c) Optical micrograph of the heterostructures. The $MoSe_2$ monolayer (indicated by the black dashed line) completely covers the WSe_2 layer, forming the heterobilayer with different stacking orders. (d) SHG from *R* and *H* stacked heterobilayers and monolayer $MoSe_2$ measured at the same condition. (e) Room temperature photoluminescence spectrum of interlayer excitons from *R* and *H* stacked regions. (f) Spatial distribution of IX energy extracted from the spectra scanned over the selected area labeled by the yellow and blue rectangles in (c).

marked by the red dashed lines. These two pieces of the monolayer labeled by *A* and *B* are separated by a bilayer marked by white dashed lines. We find that the two monolayer regions are just cleaved from the top and bottom layer of the natural bilayer. To confirm this, we prepared a heterobilayer with such a WSe_2 layer and a piece of uniform monolayer $MoSe_2$, as shown by the microscopic image in Fig. 1(c). Second harmonic generation (SHG) waves were measured from two different heterobilayer regions and the monolayer $MoSe_2$ region, respectively. The SHG intensity from the *A* and *B* regions is constructively stronger and destructively weaker than the monolayer region, respectively, indicating their stacking order is *R* type and *H* type correspondingly. The twist angle of the heterobilayer is $1.8^\circ \pm 0.6^\circ$ for the *R* stacked region and $58.2^\circ \pm 0.6^\circ$ for the *H* stacked region (see the Supplemental Material Sec. I [50] for the details of characterization).

We first characterize the stacking order dependence of the interlayer exciton energy at room temperature. The heterobilayers are excited by a nonresonant continuous wave (cw) laser with energy of 2.33 eV and a pump power of 50 μW. As shown in Fig. 1(e), the energy of photoluminescence (PL) emission from *R* and *H* stacking regions is located at 1.30 eV and 1.35 eV, respectively. This energy difference results from the different interlayer coupling strength for two stacking orders [34,35], which is consistent with results obtained from heterobilayers grown by the chemical vapor deposition method [45]. To verify the uniformity of the heterobilayers, we carried out room temperature spatial scanning PL on the two heterobilayer regions, labeled by yellow and blue rectangles, respectively. The beam diameter is about 1.5 μm, and scanning step size is 1 μm. We extract the resonance energy from the spectra measured at different locations, and plot them in Fig. 1(f). The exciton resonance energy extracted from both stacking orders is consistent over large areas, indicating the uniformity of the heterobilayers.

III. STACKING ORDER DEPENDENCE OF SPIN CONFIGURATIONS

Due to the spin-orbital coupling, both the conduction and valence band of TMD split into two bands with opposite spin. Moreover, the spin configuration is opposite for the K^+ and K^- valley because of the time reversal symmetry. Therefore, the spin alignment of the heterobilayer will be reversal for the *R* and *H* stacking regions, as shown in the schematic band structure in Figs. 2(a) and 2(e). In this section, we investigate this stacking order dependence of spin configuration using magnetoluminescence experiments at temperature of 1.6 K. As shown in Figs. 2(a) and 2(e), the lowest transitions for the two stacking orders are the spin-conserved singlet exciton and spin-nonconserved triplet excitons, respectively. The spin polarized PL spectra from the two stacking orders were obtained by exciting the heterobilayer using a circularly polarized continuous wave laser with energy of 1.96 eV and pump power of 30 nW, as shown in Figs. 2(b) and 2(f). The broader emission linewidth of the interlayer exciton from the *R* stacked region

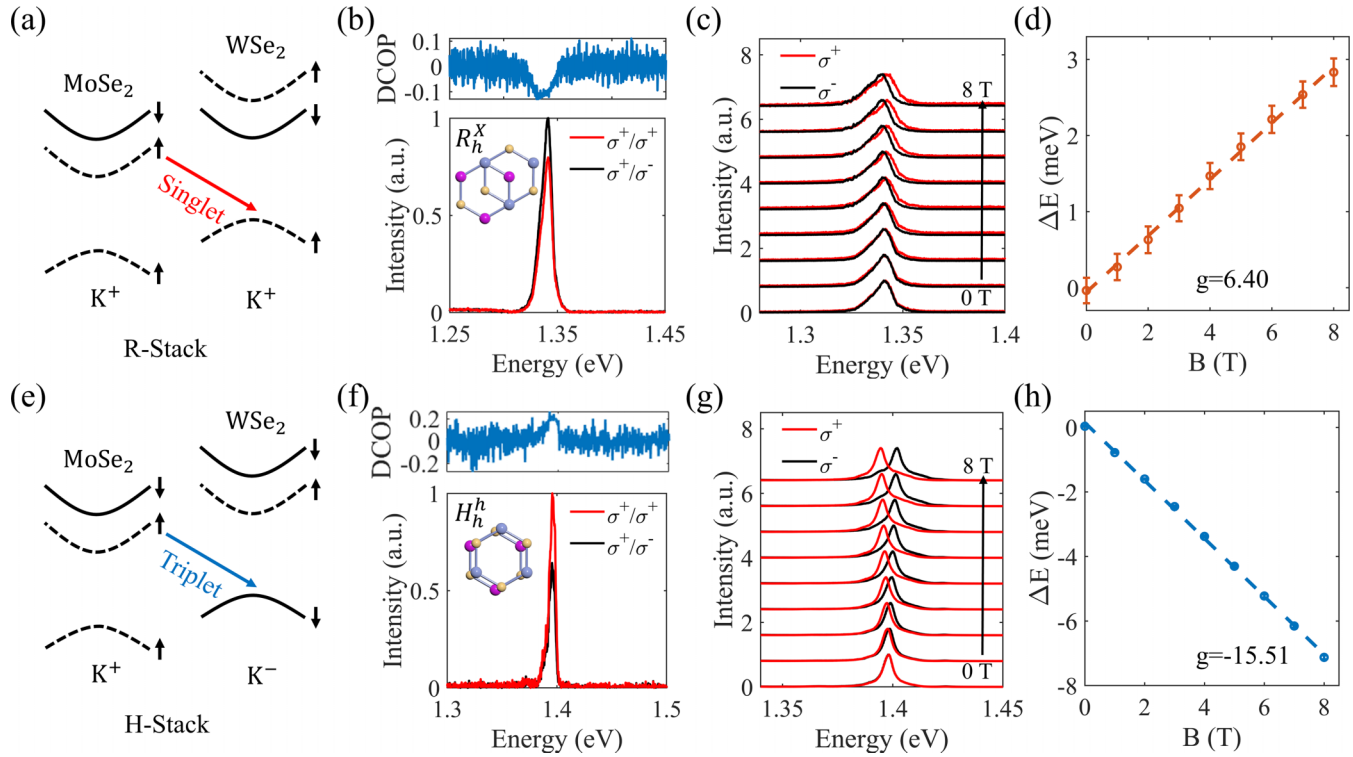

FIG. 2. Spin configurations of the heterobilayer with different stacking orders. (a), (e) Band structure of $MoSe_2/WSe_2$ heterobilayer with *R* and *H* stacking orders, where the lowest transition processes correspond to spin singlet IX (red arrow line) and triplet IX (blue arrow line), respectively. The black arrow lines represent the spin of the electron or hole. (b) Polarization-resolved PL spectra under the excitation of circularly polarized light. Inset: Exciton transition atomic registry. Top panel exhibits the degree of circular polarization (DOCP) of the IX emission. (c) Polarization-resolved spectra with increasing magnetic field applied on the out-of-plane direction. (d) Zeeman splitting of the interlayer exciton extracted from (c). *g* factors are obtained from the fits (dashed line). (f)–(h) are the similar measurements and analyses applied on the heterobilayer with *H* stacking order.

could result from the deeper moiré potential compared to that of the *H* stacked region [51,52]. For the sample with *R* stacking order, the emission exhibits stronger cross-polarized components, which is consistent with the optical selectivity for interlayer singlet exciton localized at the R_h^X atomic registry [34,35,48]. In contrast, for the *H* stacked sample, the emission with co-polarized component is stronger, which is consistent with the selection rule for interlayer triplet excitons localized at the H_h^h atomic registry [40,41,48]. To quantify the valley polarization, we define the degree of circular polarization (DOCP) as

$$\mathrm{DOCP} = \frac{I_{\sigma_+/\sigma_+} - I_{\sigma_+/\sigma_-}}{I_{\sigma_+/\sigma_+} + I_{\sigma_+/\sigma_-}}, \tag{1}$$

where I_{σ_+/σ_+} and I_{σ_+/σ_-} respectively represent the intensities of co-polarized and cross-polarized components when excited by left-circularly polarized light. DOCP is plotted as a function of energy in the top panel of Figs. 2(b) and 2(f). The opposite sign of DOCP from two different regions indicates their opposite chiral selectivity, which is in agreement with the corresponding atom registry [inset of Figs. 2(b) and 2(f)]. Such special atom registry originates from the high symmetric point within the moiré superlattice. (See Supplemental Material Fig. S4 [50] for the schematic of the full moiré superlattice.) At higher excitation power, both singlet and triplet excitons from the *H* stacked regions can be observed (see Supplemental Material Fig. S3 [50] for the polarization resolved spectra at the excitation power of 50 μW). We further conduct the polarization resolved spectroscopy with varying magnetic field applied in the out-of-plane direction of the heterobilayer. As shown in Figs. 2(c) and 2(g), the Zeeman splitting gets larger with increasing magnetic field. We fit the magnetic response of the exciton resonances using the equation

$$\Delta E = E_{\sigma_+} - E_{\sigma_-} = g\mu_B B, \tag{2}$$

where E_{σ_+} and E_{σ_-} represent the energy of exciton emission from the K^+ and K^- valleys, and μ_B is the Bohr magneton. The extracted Landé *g* factors are 6.40 and −15.51, respectively, as shown in Figs. 2(d) and 2(h). The larger amplitude of *g* factors for the exciton from the *H* stacked region results from the opposite spin quantum number of the electron and hole for the triplet IX. The stacking order dependence of *g* factors further confirms the spin singlet nature and triplet nature for the two types of excitons [41,48,53].

IV. TEMPERATURE DEPENDENCE

Although both spin singlet and triplet excitons are bright in heterobilayers, their difference in oscillator strength will influence the emission quantum yield of interlayer excitons significantly, which can be visualized in temperature-dependent PL spectra. The PL are measured within the temperature range from 1.6 K to 300 K. The heterobilayers are excited

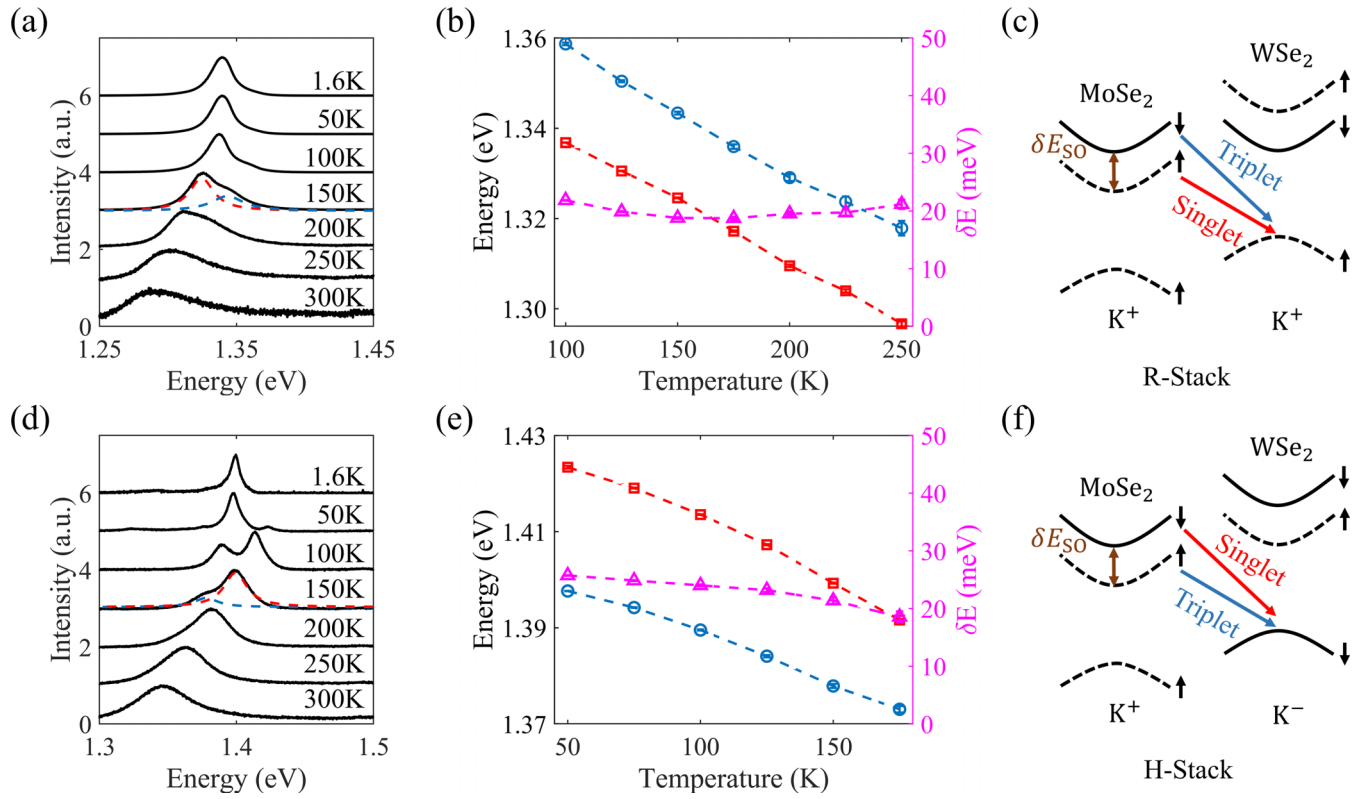

FIG. 3. Temperature dependence of heterostructure IX emission. (a) PL spectra of IX from *R*-type heterostructure at different temperatures. At higher temperature, the spectra can be well fitted by two resonances with Gaussian line shape, as indicated by the red and blue dashed lines. (b) The extracted energies by fitting the spectra in (a) at temperatures when two resonances can be well resolved. The extracted energies of the two resonances and their energy difference are shown by the blue circle, red square, and pink triangle, respectively. (c) Band structure with both spin singlet and triple excitons, corresponds to the resonances at lower and higher energies, respectively; δE_{SO} represents the conduction band splitting induced by spin-orbit coupling. (d), (e) Parallel measurements and analyses but applied to the heterobilayer with *H* stacking order.

by a cw laser with energy of 2.33 eV and a constant pump power of 25 μW. First of all, IX resonance energies from both regions exhibit redshift, which can be understood by standard temperature dependence of the semiconductor band gap [54]. Second, with increasing temperature, more emission is contributed by the higher interlayer exciton states for both *R* and *H* stacked heterobilayers. At intermediate temperatures, two resonances can be well resolved and extracted from the spectra. For example, at 150 K, the spectra can be well fitted by two resonances, represented by the red and blue dashed lines in Figs. 3(a) and 3(d). The extracted resonances and their difference δE at different temperatures are plotted in Figs. 3(b) and 3(e), where δE is around 20 meV in both stacking orders at different temperatures. This is consistent with the conduction band splitting of $MoSe_2$ (δE_{SO}) [55,56], and the two resonances correspond to the spin singlet and triple excitons in the heterobilayer. Such spin doublets in the *R* and *H* stacked heterobilayer have been obtained by chiral excitation or doping dependence spectroscopy [40,41]. Here we show that temperature can be used to drive the higher triplet and singlet states as well. The heterobilayer has been used as gain materials for nanolasers [57–59], and interlayer exciton lasers based on *R* stacked $MoSe_2/WSe_2$ heterobilayers have been demonstrated at low temperature [57,59]. Thus, it is crucial to characterize the emission quantum yield and its correlation with stacking order. As shown in Fig. 4(a), we integrate the total emission counts of the interlayer exciton measured at different temperatures. At 1.6 K, the emission intensity of the *R* stacked region is 27 times brighter than the *H* stacked region. This results from the larger oscillator strength of the spin singlet state than that of the spin triplet state [52]. With increasing temperature, more excitons are scattered outside the light cone because of stronger exciton-phonon interaction strength [60]. Therefore, both *R* and *H* stacked heterobilayers exhibit reduced emission intensity with increasing temperature. However, the reduction of emission intensity for the *R* stacked heterobilayer is continuous up to room temperature, but suppressed at 80 K for the *H* stacked heterobilayer. This sharp difference for the *R* and *H* stacked heterobilayer can be understood considering the different oscillator strength between the *R* and *H* stacked heterobilayer and the thermal population of the triplet (singlet) state for the *H* (*R*) stacked heterobilayer. As schematically shown in Fig. 4(c), for the *H* stacked heterobilayer, the spin singlet exciton with larger oscillator strength will get thermally populated with increasing temperature, and thereby compensates the reduction of the quantum yield induced by the thermally activated nonradiative process. In contrast, for the *R* stacked heterobilayer, the thermal population of the higher triplet exciton with lower radiative rate will enhance the reduction of emission quantum

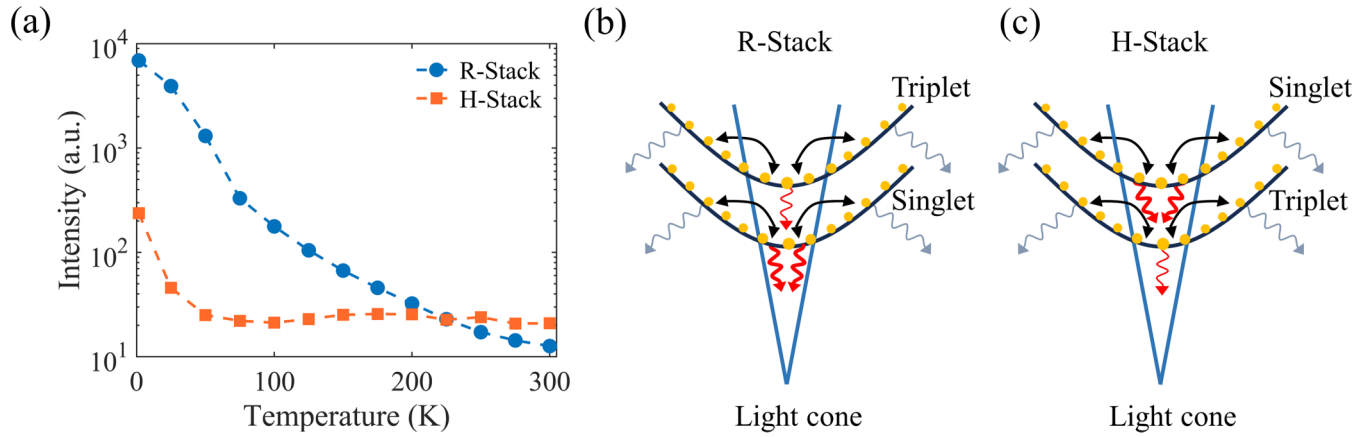

FIG. 4. Temperature dependence of emission intensity. (a) Integrated emission intensity of IX from *R* and *H* stacked heterobilayer as a function of temperature. (b), (c) Schematics showing the emission dynamics for singlet and triplet excitons in *R* and *H* stacked heterobilayers, respectively. The red wave lines represent the radiative emission from IX within the light cone, where the thicker and thinner wave line indicate the stronger and weaker emission rate from singlet and triple excitons, respectively. The gray wave line outside the light cone represents the nonradiative process, which can be enhanced by the phonon-assisted scattering represented by the black double-arrow lines.

yield, as shown in Fig. 4(b). We also apply coupled rate equations to quantitatively model the temperature dependence of emission intensity for both *R* and *H* stacked regions. (See Supplemental Material Sec. II [50] for details.) Our results indicate that *R* and *H* stacked $MoSe_2/WSe_2$ are better gain materials at low and room temperatures, respectively, and quantitative modeling of the correlation between the emission quantum yield and stacking orders needs microscopic theories [61,62].

V. CONCLUSION

Stacking order dependence of interlayer excitons is systematically studied in a $MoSe_2/WSe_2$ heterobilayer that simultaneously hosts two different stacking orders. The impact of stacking order is manifested as the transition energy, valley polarization, and magnetic responses of interlayer excitons. Interestingly, the temperature dependence of quantum yield for interlayer excitons is significantly correlated to stacking orders as well, which provides understanding for designing light harvesting devices based on heterobilayers. Such a platform can be readily extended to explore other stacking order dependencies of excitons, such as exciton diffusions [32,33,63,64], interlayer hybridization [38], and strong correlation of excitons [22,27].

ACKNOWLEDGMENTS

The work is supported by National Key R&D Program of China (Grant No. 2022YFA1204700), the National Natural Science Foundation of China (Grants No. 62175207, No. 92250301, and No. 12304347), the Shccig-Qinling Program, Fundamental Research Funds for the Central Universities Grant No. 20720210004, and Natural Science Foundation of Fujian Province under Grant No. 2021J01007.

[1] N. P. Wilson, W. Yao, J. Shan, and X. Xu, Excitons and emergent quantum phenomena in stacked 2D semiconductors, Nature (London) **599**, 383 (2021).
[2] E. C. Regan, D. Wang, E. Y. Paik, Y. Zeng, L. Zhang, J. Zhu, A. H. MacDonald, H. Deng, and F. Wang, Emerging exciton physics in transition metal dichalcogenide heterobilayers, Nat. Rev. Mater. **7**, 778 (2022).
[3] D. Huang, J. Choi, C.-K. Shih, and X. Li, Excitons in semiconductor moiré superlattices, Nat. Nanotechnol. **17**, 227 (2022).
[4] K. F. Mak and J. Shan, Semiconductor moiré materials, Nat. Nanotechnol. **17**, 686 (2022).
[5] L. Du, M. R. Molas, Z. Huang, G. Zhang, F. Wang, and Z. Sun, Moiré photonics and optoelectronics, Science **379**, eadg0014 (2023).
[6] C. Jin, E. C. Regan, A. Yan, M. I. B. Utama, D. Wang, S. Zhao, Y. Qin, S. Yang, Z. Zheng, S. Shi *et al.*, Observation of moiré excitons in WSe_2/WS_2 heterostructure superlattices, Nature (London) **567**, 76 (2019).
[7] K. Tran, G. Moody, F. Wu, X. Lu, J. Choi, K. Kim, A. Rai, D. A. Sanchez, J. Quan, A. Singh *et al.*, Evidence for moiré excitons in van der Waals heterostructures, Nature (London) **567**, 71 (2019).
[8] K. L. Seyler, P. Rivera, H. Yu, N. P. Wilson, E. L. Ray, D. G. Mandrus, J. Yan, W. Yao, and X. Xu, Signatures of moiré-trapped valley excitons in $MoSe_2/WSe_2$ heterobilayers, Nature (London) **567**, 66 (2019).
[9] E. M. Alexeev, D. A. Ruiz-Tijerina, M. Danovich, M. J. Hamer, D. J. Terry, P. K. Nayak, S. Ahn, S. Pak, J. Lee, J. I. Sohn *et al.*, Resonantly hybridized excitons in moiré superlattices in van der Waals heterostructures, Nature (London) **567**, 81 (2019).
[10] C. Jin, E. C. Regan, D. Wang, M. Iqbal Bakti Utama, C.-S. Yang, J. Cain, Y. Qin, Y. Shen, Z. Zheng, K. Watanabe *et al.*,

Identification of spin, valley and moiré quasi-angular momentum of interlayer excitons, Nat. Phys. **15**, 1140 (2019).

[11] T. I. Andersen, G. Scuri, A. Sushko, K. De Greve, J. Sung, Y. Zhou, D. S. Wild, R. J. Gelly, H. Heo, D. Bérubé *et al.*, Excitons in a reconstructed moiré potential in twisted WSe_2/WSe_2 homobilayers, Nat. Mater. **20**, 480 (2021).

[12] F. Wu, T. Lovorn, E. Tutuc, and A. H. MacDonald, Hubbard model physics in transition metal dichalcogenide moiré bands, Phys. Rev. Lett. **121**, 026402 (2018).

[13] E. C. Regan, D. Wang, C. Jin, M. I. Bakti Utama, B. Gao, X. Wei, S. Zhao, W. Zhao, Z. Zhang, K. Yumigeta *et al.*, Mott and generalized Wigner crystal states in WSe_2/WS_2 moiré superlattices, Nature (London) **579**, 359 (2020).

[14] Y. Tang, L. Li, T. Li, Y. Xu, S. Liu, K. Barmak, K. Watanabe, T. Taniguchi, A. H. MacDonald, J. Shan *et al.*, Simulation of Hubbard model physics in WSe_2/WS_2 moiré superlattices, Nature (London) **579**, 353 (2020).

[15] Y. Xu, S. Liu, D. A. Rhodes, K. Watanabe, T. Taniguchi, J. Hone, V. Elser, K. F. Mak, and J. Shan, Correlated insulating states at fractional fillings of moiré superlattices, Nature (London) **587**, 214 (2020).

[16] Y. Shimazaki, I. Schwartz, K. Watanabe, T. Taniguchi, M. Kroner, and A. Imamoğlu, Strongly correlated electrons and hybrid excitons in a moiré heterostructure, Nature (London) **580**, 472 (2020).

[17] X. Huang, T. Wang, S. Miao, C. Wang, Z. Li, Z. Lian, T. Taniguchi, K. Watanabe, S. Okamoto, D. Xiao *et al.*, Correlated insulating states at fractional fillings of the WS_2/WSe_2 moiré lattice, Nat. Phys. **17**, 715 (2021).

[18] E. Liu, T. Taniguchi, K. Watanabe, N. M. Gabor, Y.-T. Cui, and C. H. Lui, Excitonic and valley-polarization signatures of fractional correlated electronic phases in a WSe_2/WS_2 moiré superlattice, Phys. Rev. Lett. **127**, 037402 (2021).

[19] C. Jin, Z. Tao, T. Li, Y. Xu, Y. Tang, J. Zhu, S. Liu, K. Watanabe, T. Taniguchi, J. C. Hone *et al.*, Stripe phases in WSe_2/WS_2 moiré superlattices, Nat. Mater. **20**, 940 (2021).

[20] J. Gu, L. Ma, S. Liu, K. Watanabe, T. Taniguchi, J. C. Hone, J. Shan, and K. F. Mak, Dipolar excitonic insulator in a moiré lattice, Nat. Phys. **18**, 395 (2022).

[21] D. Chen, Z. Lian, X. Huang, Y. Su, M. Rashetnia, L. Ma, L. Yan, M. Blei, L. Xiang, T. Taniguchi *et al.*, Excitonic insulator in a heterojunction moiré superlattice, Nat. Phys. **18**, 1171 (2022).

[22] R. Xiong, J. H. Nie, S. L. Brantly, P. Hays, R. Sailus, K. Watanabe, T. Taniguchi, S. Tongay, and C. Jin, Correlated insulator of excitons in WSe_2/WS_2 moiré superlattices, Science **380**, 860 (2023).

[23] Y. Zeng, Z. Xia, K. Kang, J. Zhu, P. Knüppel, C. Vaswani, K. Watanabe, T. Taniguchi, K. F. Mak, and J. Shan, Thermodynamic evidence of fractional Chern insulator in moiré $MoTe_2$, Nature (London) **622**, 69 (2023).

[24] F. Xu, Z. Sun, T. Jia, C. Liu, C. Xu, C. Li, Y. Gu, K. Watanabe, T. Taniguchi, B. Tong *et al.*, Observation of integer and fractional quantum anomalous Hall effects in twisted bilayer $MoTe_2$, Phys. Rev. X **13**, 031037 (2023).

[25] H. Park, J. Cai, E. Anderson, Y. Zhang, J. Zhu, X. Liu, C. Wang, W. Holtzmann, C. Hu, Z. Liu *et al.*, Observation of fractionally quantized anomalous Hall effect, Nature (London) **622**, 74 (2023).

[26] J. Cai, E. Anderson, C. Wang, X. Zhang, X. Liu, W. Holtzmann, Y. Zhang, F. Fan, T. Taniguchi, K. Watanabe *et al.*, Signatures of fractional quantum anomalous Hall states in twisted $MoTe_2$, Nature (London) **622**, 63 (2023).

[27] Z. Lian, Y. Meng, L. Ma, I. Maity, L. Yan, Q. Wu, X. Huang, D. Chen, X. Chen, X. Chen *et al.*, Valley-polarized excitonic Mott insulator in WS_2/WSe_2 moiré superlattice, Nat. Phys. **20**, 34 (2024).

[28] P. K. Nayak, Y. Horbatenko, S. Ahn, G. Kim, J.-U. Lee, K. Y. Ma, A.-R. Jang, H. Lim, D. Kim, S. Ryu *et al.*, Probing evolution of twist-angle-dependent interlayer excitons in $MoSe_2/WSe_2$ van der Waals heterostructures, ACS Nano **11**, 4041 (2017).

[29] L. Zhang, Z. Zhang, F. Wu, D. Wang, R. Gogna, S. Hou, K. Watanabe, T. Taniguchi, K. Kulkarni, T. Kuo *et al.*, Twist-angle dependence of moiré excitons in $WS_2/MoSe_2$ heterobilayers, Nat. Commun. **11**, 5888 (2020).

[30] J. Choi, M. Florian, A. Steinhoff, D. Erben, K. Tran, D. S. Kim, L. Sun, J. Quan, R. Claassen, S. Majumder *et al.*, Twist angle-dependent interlayer exciton lifetimes in van der Waals heterostructures, Phys. Rev. Lett. **126**, 047401 (2021).

[31] E. Barré, O. Karni, E. Liu, A. L. O'Beirne, X. Chen, H. B. Ribeiro, L. Yu, B. Kim, K. Watanabe, T. Taniguchi *et al.*, Optical absorption of interlayer excitons in transition-metal dichalcogenide heterostructures, Science **376**, 406 (2022).

[32] L. Yuan, B. Zheng, J. Kunstmann, T. Brumme, A. B. Kuc, C. Ma, S. Deng, D. Blach, A. Pan, and L. Huang, Twist-angle-dependent interlayer exciton diffusion in WS_2/WSe_2 heterobilayers, Nat. Mater. **19**, 617 (2020).

[33] J. Choi, W.-T. Hsu, L.-S. Lu, L. Sun, H.-Y. Cheng, M.-H. Lee, J. Quan, K. Tran, C.-Y. Wang, M. Staab *et al.*, Moiré potential impedes interlayer exciton diffusion in van der Waals heterostructures, Sci. Adv. **6**, eaba8866 (2020).

[34] H. Yu, G.-B. Liu, J. Tang, X. Xu, and W. Yao, Moiré excitons: From programmable quantum emitter arrays to spin-orbit–coupled artificial lattices, Sci. Adv. **3**, e1701696 (2017).

[35] F. Wu, T. Lovorn, and A. H. MacDonald, Theory of optical absorption by interlayer excitons in transition metal dichalcogenide heterobilayers, Phys. Rev. B **97**, 035306 (2018).

[36] P. Nagler, M. V. Ballottin, A. A. Mitioglu, F. Mooshammer, N. Paradiso, C. Strunk, R. Huber, A. Chernikov, P. C. Christianen, C. Schüller *et al.*, Giant magnetic splitting inducing near-unity valley polarization in van der Waals heterostructures, Nat. Commun. **8**, 1551 (2017).

[37] M. Förg, A. S. Baimuratov, S. Y. Kruchinin, I. A. Vovk, J. Scherzer, J. Förste, V. Funk, K. Watanabe, T. Taniguchi, and A. Högele, Moiré excitons in $MoSe_2$-WSe_2 heterobilayers and heterotrilayers, Nat. Commun. **12**, 1656 (2021).

[38] D. A. Ruiz-Tijerina and V. I. Fal'ko, Interlayer hybridization and moiré superlattice minibands for electrons and excitons in heterobilayers of transition-metal dichalcogenides, Phys. Rev. B **99**, 125424 (2019).

[39] Y. Tang, J. Gu, S. Liu, K. Watanabe, T. Taniguchi, J. Hone, K. F. Mak, and J. Shan, Tuning layer-hybridized moiré excitons by the quantum-confined Stark effect, Nat. Nanotechnol. **16**, 52 (2021).

[40] L. Zhang, R. Gogna, G. W. Burg, J. Horng, E. Paik, Y.-H. Chou, K. Kim, E. Tutuc, and H. Deng, Highly valley-polarized singlet and triplet interlayer excitons in van der Waals heterostructure, Phys. Rev. B **100**, 041402(R) (2019).

[41] A. Y. Joe, L. A. Jauregui, K. Pistunova, A. M. MierValdivia, Z. Lu, D. S. Wild, G. Scuri, K. DeGreve, R. J. Gelly, Y. Zhou,

J. Sung, A. Sushko, T. Taniguchi, K. Watanabe, D. Smirnov, M. D. Lukin, H. Park, and P. Kim, Electrically controlled emission from singlet and triplet exciton species in atomically thin light-emitting diodes, Phys. Rev. B **103**, L161411 (2021).

[42] L. Yu, K. Pistunova, J. Hu, K. Watanabe, T. Taniguchi, and T. F. Heinz, Observation of quadrupolar and dipolar excitons in a semiconductor heterotrilayer, Nat. Mater. **22**, 1485 (2023).

[43] Z. Lian, D. Chen, L. Ma, Y. Meng, Y. Su, L. Yan, X. Huang, Q. Wu, X. Chen, M. Blei *et al.*, Quadrupolar excitons and hybridized interlayer Mott insulator in a trilayer moiré superlattice, Nat. Commun. **14**, 4604 (2023).

[44] W. Li, Z. Hadjri, L. M. Devenica, J. Zhang, S. Liu, J. Hone, K. Watanabe, T. Taniguchi, A. Rubio, and A. Srivastava, Quadrupolar-dipolar excitonic transition in a tunnel-coupled van der Waals heterotrilayer, Nat. Mater. **22**, 1478 (2023).

[45] W.-T. Hsu, L.-S. Lu, P.-H. Wu, M.-H. Lee, P.-J. Chen, P.-Y. Wu, Y.-C. Chou, H.-T. Jeng, L.-J. Li, M.-W. Chu *et al.*, Negative circular polarization emissions from $WSe_2/MoSe_2$ commensurate heterobilayers, Nat. Commun. **9**, 1356 (2018).

[46] N. Leisgang, S. Shree, I. Paradisanos, L. Sponfeldner, C. Robert, D. Lagarde, A. Balocchi, K. Watanabe, T. Taniguchi, X. Marie *et al.*, Giant Stark splitting of an exciton in bilayer MoS_2, Nat. Nanotechnol. **15**, 901 (2020).

[47] J. Sung, Y. Zhou, G. Scuri, V. Zólyomi, T. I. Andersen, H. Yoo, D. S. Wild, A. Y. Joe, R. J. Gelly, H. Heo *et al.*, Broken mirror symmetry in excitonic response of reconstructed domains in twisted $MoSe_2/MoSe_2$ bilayers, Nat. Nanotechnol. **15**, 750 (2020).

[48] S. Zhao, Z. Li, X. Huang, A. Rupp, J. Göser, I. A. Vovk, S. Y. Kruchinin, K. Watanabe, T. Taniguchi, I. Bilgin *et al.*, Excitons in mesoscopically reconstructed moiré heterostructures, Nat. Nanotechnol. **18**, 572 (2023).

[49] X. Huang, X. Han, Y. Dai, X. Xu, J. Yan, M. Huang, P. Ding, D. Zhang, H. Chen, V. Laxmi *et al.*, Recent progress on fabrication and flat-band physics in 2D transition metal dichalcogenides moiré superlattices, J. Semicond. **44**, 011901 (2023).

[50] See Supplemental Material at http://link.aps.org/supplemental/10.1103/PhysRevB.110.045412 for additional details including twist angle of heterojunction, simulation of temperature dependence of emission intensity, polarization resolved spectra of singlet and triplet excitons for the *H* stacked regions, and moiré superlattice schematic.

[51] P. Rivera, J. R. Schaibley, A. M. Jones, J. S. Ross, S. Wu, G. Aivazian, P. Klement, K. Seyler, G. Clark, N. J. Ghimire *et al.*, Observation of long-lived interlayer excitons in monolayer $MoSe_2/WSe_2$ heterostructures, Nat. Commun. **6**, 6242 (2015).

[52] H. Yu, G.-B. Liu, and W. Yao, Brightened spin-triplet interlayer excitons and optical selection rules in van der Waals heterobilayers, 2D Mater. **5**, 035021 (2018).

[53] T. Woźniak, P. E. Faria Junior, G. Seifert, A. Chaves, and J. Kunstmann, Exciton *g* factors of van der Waals heterostructures from first-principles calculations, Phys. Rev. B **101**, 235408 (2020).

[54] H. Fan, Temperature dependence of the energy gap in semiconductors, Phys. Rev. **82**, 900 (1951).

[55] G.-B. Liu, D. Xiao, Y. Yao, X. Xu, and W. Yao, Electronic structures and theoretical modelling of two-dimensional group-VIB transition metal dichalcogenides, Chem. Soc. Rev. **44**, 2643 (2015).

[56] S. Larentis, H. C. P. Movva, B. Fallahazad, K. Kim, A. Behroozi, T. Taniguchi, K. Watanabe, S. K. Banerjee, and E. Tutuc, Large effective mass and interaction-enhanced Zeeman splitting of *K*-valley electrons in $MoSe_2$, Phys. Rev. B **97**, 201407(R) (2018).

[57] E. Y. Paik, L. Zhang, G. W. Burg, R. Gogna, E. Tutuc, and H. Deng, Interlayer exciton laser of extended spatial coherence in atomically thin heterostructures, Nature (London) **576**, 80 (2019).

[58] Y. Liu, H. Fang, A. Rasmita, Y. Zhou, J. Li, T. Yu, Q. Xiong, N. Zheludev, J. Liu, and W. Gao, Room temperature nanocavity laser with interlayer excitons in 2D heterostructures, Sci. Adv. **5**, eaav4506 (2019).

[59] C. Qian, M. Troue, J. Figueiredo, P. Soubelet, V. Villafañe, J. Beierlein, S. Klembt, A. V. Stier, S. Höfling, A. W. Holleitner *et al.*, Lasing of moiré trapped $MoSe_2/WSe_2$ interlayer excitons coupled to a nanocavity, Sci. Adv. **10**, eadk6359 (2024).

[60] X.-X. Zhang, Y. You, S. Y. F. Zhao, and T. F. Heinz, Experimental evidence for dark excitons in monolayer WSe_2, Phys. Rev. Lett. **115**, 257403 (2015).

[61] C. Hu, M. H. Naik, Y.-H. Chan, and S. G. Louie, Excitonic interactions and mechanism for ultrafast interlayer photoexcited response in van der Waals heterostructures, Phys. Rev. Lett. **131**, 236904 (2023).

[62] R. Perea-Causin, S. Brem, O. Schmidt, and E. Malic, Trion photoluminescence and trion stability in atomically thin semiconductors, Phys. Rev. Lett. **132**, 036903 (2024).

[63] Q. Tan, A. Rasmita, Z. Zhang, K. Novoselov, and W.-B. Gao, Signature of cascade transitions between interlayer excitons in a moiré superlattice, Phys. Rev. Lett. **129**, 247401 (2022).

[64] E. Wietek, M. Florian, J. Göser, T. Taniguchi, K. Watanabe, A. Högele, M. M. Glazov, A. Steinhoff, and A. Chernikov, Nonlinear and negative effective diffusivity of interlayer excitons in moiré-free heterobilayers, Phys. Rev. Lett. **132**, 016202 (2024).